

# AOCIL: Exemplar-free Analytic Online Class Incremental Learning with Low Time and Resource Consumption

Huiping Zhuang<sup>1</sup> Yuchen Liu<sup>2</sup> Run He<sup>1</sup> Kai Tong<sup>1</sup> Ziqian Zeng<sup>1</sup> Cen Chen<sup>3</sup> Yi Wang<sup>4</sup> Lap-Pui Chau<sup>4</sup>

## Abstract

Online Class Incremental Learning (OCIL) aims to train the model in a task-by-task manner, where data arrive in mini-batches at a time while previous data are not accessible. A significant challenge is known as Catastrophic Forgetting, i.e., loss of the previous knowledge on old data. To address this, replay-based methods show competitive results but invade data privacy, while exemplar-free methods protect data privacy but struggle for accuracy. In this paper, we proposed an exemplar-free approach—Analytic Online Class Incremental Learning (AOCIL). Instead of back-propagation, we design the Analytic Classifier (AC) updated by recursive least square, cooperating with a frozen backbone. AOCIL simultaneously achieves high accuracy, low resource consumption and data privacy protection. We conduct massive experiments on four existing benchmark datasets, and the results demonstrate the strong capability of handling OCIL scenarios. Codes will be ready at <https://github.com/ZHUANGHP/Analytic-continual-learning>

## 1. Introduction

Class Incremental Learning (CIL) updates the model incrementally in a task-by-task manner with new class instances only. Traditional CIL most plan for static offline datasets which historical data is accessible. However, with the rapid increase of social medias and mobile devices, massive amount of image data have been produced online in a streaming fashion, and render training models on static data

<sup>\*</sup>Equal contribution <sup>1</sup>Shien-Ming Wu School of Intelligent Engineering, South China University of Technology, Guangzhou, China <sup>2</sup>Department of Mechanic Engineering, The University of Hong Kong, Hong Kong <sup>3</sup>School of Future Technology, South China University of Technology, Guangzhou, China <sup>4</sup>Department of Electrical and Electronic Engineering, The Hong Kong Polytechnic University, Hong Kong. Correspondence to: Huiping Zhuang <hpzhuang@scut.edu.cn>.

less applicable. To address this, Online Class Incremental Learning (OCIL) is developed taking an online constraint in addition to the existing CIL setting. OCIL is a more challenging CIL setting in which data come in mini-batches, and the model is trained only in one epoch (i.e., learning from one pass data stream) (He et al., 2020). The model is supposed to achieve high accuracy, fast training time, and low resource consumption (Mai et al., 2021).

However, CIL techniques (including OCIL) suffer from Catastrophic Forgetting (CF) (McCloskey & Cohen, 1989), also known as the erosion of previous knowledge when new data are introduced. The problem becomes more severe in online scenarios since the model can only see data once. Two major factors contribute to CF: (1) Using the loss function to update the whole network leads to uncompleted feature capturing and diminished global representation (Guo et al., 2022). (2) Using back-propagation to adjust linear classifier results in *recency bias*, which is a significantly imbalanced weight distribution, showing preference only on current learning data (Hou et al., 2019).

To address CF in an online setting, replay-based methods (Gu et al., 2022; Lin et al., 2023) are the mainstream solution by preserving old exemplars and revisiting them in new tasks. This strategy has strong performance but invades data privacy. There exist exemplar-free methods (Kirkpatrick et al., 2017; Li & Hoiem, 2017) that protect data privacy but show less competitive results.

Recently, Analytic Learning (AL) (Zhuang et al., 2022) methods emerged as an exemplar-free branch, delivering encouraging outcomes. AL-based methods pinpoint the iterative back-propagation as the main factor behind catastrophic forgetting and seek to address it through linear recursive strategies. Remarkably, for the first time, these methods achieve outcomes comparable to those utilizing replay-based techniques.

There are two limitations in existing AL-based methods: (1) Multiple iterations of base training are needed when the model is applied. Subsequently, the acquired knowledge is encoded into a *regularized feature autocorrelation matrix* by analytic re-alignment. The incremental learning phase then unfolds, utilizing the recursive least squares method

for updates. This pattern is repeated when the dataset is switched, significantly elevating the temporal cost in an online scenario. (2) Classic AL-based methods demand data aggregation from a single task, facilitating analytic learning in one fell swoop. This process increases GPU usage and is unsuitable for online contexts where data for each task is presented as mini-batches.

To address those limitations, we propose Analytic Online Class Incremental Learning (AOCIL) that learns online batch-wise data streams. The AOCIL consists of a frozen pre-trained Vision Transformer (ViT) as a backbone network and an Analytic Classifier (AC). The frozen backbone is capable of countering the uncompleted feature representation caused by using the loss function to update and replace the time-consuming base training. The AC is updated by recursive least square rather than back-propagation to solve recency bias and decrease calculation. Therefore, AOCIL is an exemplar-free countermeasure to CF and reduces resource consumption since the backbone model is frozen and only the classifier is updated.

Our main contributions can be concluded as follows:

- We present the AOCIL, an exemplar-free technique that achieves high accuracy, data privacy protection, and low resource consumption together for OCIL problems.
- AOCIL redefines the OCIL problem into a recursive least square manner and is updated in a batch-wise manner.
- AOCIL introduces a framework of frozen ViT and recursively updated AC to alleviate CF.
- We conduct massive experiments on four benchmark datasets with baselines. The results demonstrate that AOCIL is better than other exemplar-free methods and surpasses several replay-based methods while we use minimal time and memory.

## 2. Related Work

**Online Class Incremental Learning** focuses on extracting knowledge from one pass data stream with new classes in the new task. Time and memory consumption requirements are particularly critical in OCIL, given the fast and large nature of online data streams (He et al., 2020).

**Replay-based methods** (Shim et al., 2021; Mai et al., 2021; Lin et al., 2023; Gu et al., 2022; Rebuffi et al., 2017; Hayes et al., 2019; Aljundi et al., 2019b; Guo et al., 2022; Hou et al., 2019; Zhang et al., 2022; Wang et al., 2022; 2023; Aljundi et al., 2019a; Wei et al., 2023; Lee et al., 2023) are mainstream solutions for OCIL problems by preserving historical exemplars and using them in new tasks. The accuracy is better than exemplar-free methods', but the time and memory consumption is higher. In addition, using

exemplars leads to data privacy concerns.

**Analytic Learning** (AL), also referred to as pseudoinverse learning (Guo et al., 2001), emerges as a solution to the pitfalls of back-propagation by recursive least square. Analytic Learning's computational intensity is demanding since the entire dataset is processed. The obstacle is solved by the block-wise recursive Moore-Penrose algorithm (Zhuang et al., 2021), which achieves equivalent precision with joint learning.

**Exemplar-free methods** can be categorized into regularization-based, prototype-based, and recently emerged AL-based methods.

• **Regularization-based methods** (Li & Hoiem, 2017; Kirkpatrick et al., 2017) apply constraints on the loss function or change the gradients to preserve knowledge. These solutions reduce resource consumption and protect data privacy. However, the results are not competitive in the OCIL scenario.

• **Prototype-based methods** (Zhu et al., 2021; 2022; Petit et al., 2023) mitigate CF by augmenting the prototypes of features to classify old classes or generating psudofeatures of old classes from new representations.

• **AL-based methods** represent a new branch of the CIL community and show great potential in the OCIL scenario. Analytic Class Incremental Learning (ACIL) (Zhuang et al., 2022) is the first approach that applies Analytic Learning to the CIL problem. The ACIL achieves a competitive performance in the offline CIL scenario. Gaussian Kernel Embedded Analytic Learning (GKEAL) (Zhuang et al., 2023), following the ACIL, focuses on solving CF in the few-shot scenario by adopting the kernel method.

## 3. Methodology

### 3.1. Proposed Framework

Our AOCIL framework consists of two modules:

**Frozen Pre-trained ViT.** The ViT generates *class tokens* (i.e., vectors that capture features of images) that have global information and stronger representational power compared to the feature embeddings derived from convolutional neural networks (Raghu et al., 2021). The class tokens are typically in high dimension, which is desirable for AL (Zhuang et al., 2022). Freezing the backbone avoids selective learning caused by loss function, which prioritizes features that are easiest to learn rather than the most representative (Guo et al., 2022).

**Analytic Classifier.** By recursive least square, AC avoids the *recency bias* because the recursive update leads to identical results to joint learning on all data. Therefore, every sample of data is equally treated. Additionally, pairing AC

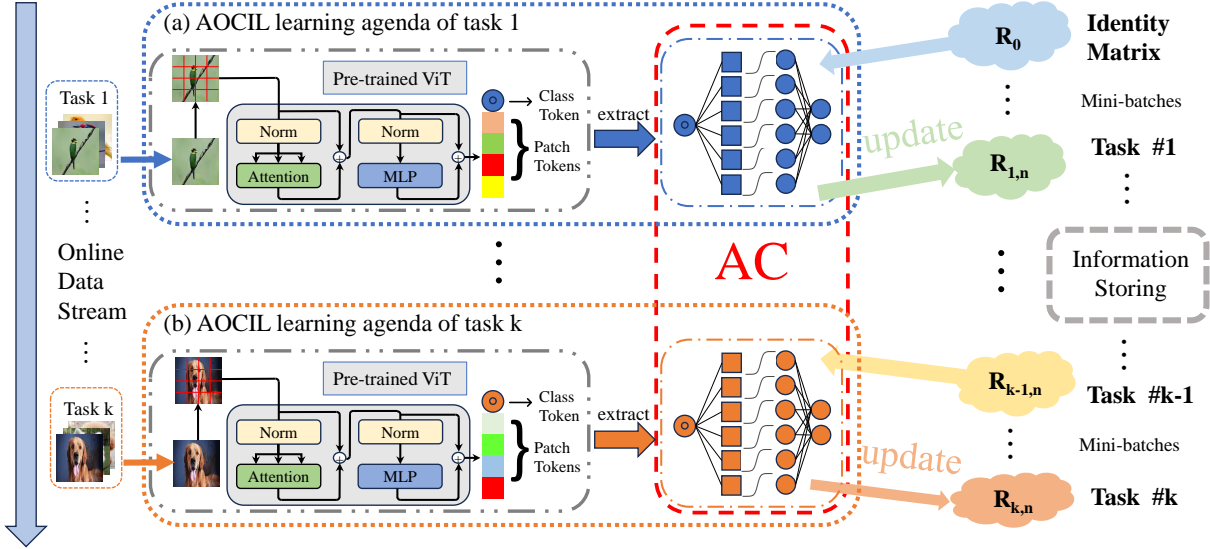


Figure 1. An overview of the proposed AOCIL.  $\mathbf{R}_0$  is initialized as an identity matrix. The pre-trained and frozen ViT extracts the class tokens from online data streams. AC randomly projects and normalizes the tokens to higher dimensional space as new activations. New mini-batches are learned in a recursive manner. Only  $\mathbf{R}_{k,i}$  and the linear classifier’s weight matrix are recursively updated throughout the whole framework without preserving historical exemplars.

with a frozen ViT significantly reduces the number of parameters that need training, enhancing the model’s efficiency.

### 3.2. Learning Agenda

The overview is shown in Figure 1. Given dataset  $\{\mathbf{X}_k^{\text{train}}, \mathbf{Y}_k^{\text{train}}\}_1^K$  be the training set of task  $k$  ( $k = 1, 2, \dots, K$ ). Every task is divided into  $n$  mini-batches. We denote  $\{\mathbf{X}_{k,i}^{\text{train}}, \mathbf{Y}_{k,i}^{\text{train}}\}$ , as the  $i$  mini-batch ( $i=1, 2, \dots, n$ ) of training set of task  $k$ . The learning agenda has two stages:

#### Acquiring Activation by ViT

When the batch 1 of task 1 (i.e.,  $\{\mathbf{X}_{1,1}^{\text{train}}, \mathbf{Y}_{1,1}^{\text{train}}\}$ ) comes, the first step is to extract class token matrix  $\mathbf{X}_{1,1}^{\text{cls}}$  from  $\mathbf{X}_{1,1}^{\text{train}}$  with pre-trained and frozen  $f_{\text{ViT}}$ :

$$\mathbf{X}_{1,1}^{\text{cls}} = f_{\text{ViT}}(\mathbf{X}_{1,1}^{\text{train}}) \quad (1)$$

and the AC takes  $\mathbf{X}_{1,1}^{\text{cls}}$  as input and computes the activation matrix  $\mathbf{X}_{1,1}^{(a)}$  by the equation:

$$\mathbf{X}_{1,1}^{(a)} = f_{\text{act}}(f_{\text{proj}}(\mathbf{X}_{1,1}^{\text{cls}})) \quad (2)$$

where  $f_{\text{act}}$  is the activation function and  $f_{\text{proj}}$  is the random projection to higher dimension. We adopt Sigmoid as the activation function to add non-linear information. For the projection matrix, we draw every element from a normal distribution since Analytic Learning requires more parameters for the calculation to achieve maximum performance (Zhuang et al., 2022). This technique is able to extract useful information for classification problems.

#### Updating AC Recursively

We map the activation matrix  $\mathbf{X}_{1,1}^{(a)}$  to the one-hot label matrix  $\mathbf{Y}_{1,1}^{\text{train}}$  using a linear regression procedure via solving

$$\underset{\mathbf{W}^{(1,1)}}{\text{argmin}} \|\mathbf{Y}_{1,1}^{\text{train}} - \mathbf{X}_{1,1}^{(a)} \mathbf{W}^{(1,1)}\|_F^2 + \gamma \|\mathbf{W}^{(1,1)}\|_F^2. \quad (3)$$

$\mathbf{W}^{(1,1)}$  is the weight matrix of the linear classifier of batch 1 of task 1.  $\|\cdot\|_F$  represents the Frobenius norm and  $\gamma$  is the regularization term. Then we have the expected weight matrix by optimizing Equation 3

$$\hat{\mathbf{W}}^{(1,1)} = \left( \mathbf{X}_{1,1}^{(a)\text{T}} \mathbf{X}_{1,1}^{(a)} + \gamma \mathbf{I} \right)^{-1} \mathbf{X}_{1,1}^{(a)\text{T}} \mathbf{Y}_{1,1}^{\text{train}}. \quad (4)$$

When the rest of the batches (i.e.,  $i=2, \dots, n$ ) are given in task 1, the one-hot label matrix and activation matrix of the whole task become

$$\mathbf{Y}_1^{\text{train}} = \begin{bmatrix} \mathbf{Y}_{1,1}^{\text{train}} & \cdots & \mathbf{0} \\ \vdots & \ddots & \vdots \\ \mathbf{0} & \cdots & \mathbf{Y}_{1,n}^{\text{train}} \end{bmatrix}, \quad \mathbf{X}_1^{(a)} = \begin{bmatrix} \mathbf{X}_{1,1}^{(a)} \\ \vdots \\ \mathbf{X}_{1,n}^{(a)} \end{bmatrix}. \quad (5)$$

The final optimal estimation of the weight matrix for task 1 can be written as

$$\hat{\mathbf{W}}^{(1,n)} = \left( \sum_{i=1}^n \mathbf{X}_{1,i}^{(a)\text{T}} \mathbf{X}_{1,i}^{(a)} + \gamma \mathbf{I} \right)^{-1} \begin{bmatrix} \mathbf{X}_{1,1}^{(a)\text{T}} \mathbf{Y}_{1,1}^{\text{train}} \\ \vdots \\ \mathbf{X}_{1,n}^{(a)\text{T}} \mathbf{Y}_{1,n}^{\text{train}} \end{bmatrix}. \quad (6)$$

Equation 6 indicates the joint learning result by the least square method, which is not suitable in online scenarios

**Algorithm 1** Analytic Online Class Incremental Learning

---

**Input:** Mini-batch  $\{X_{k,i}^{\text{train}}, Y_{k,i}^{\text{train}}\}_{1,1}^{K,n}$

**Initialization:** Identity matrix  $\mathbf{R}_0$ ; Null matrix  $\mathbf{W}^{(0)}$  and pre-trained frozen ViT

**for**  $k = 1$  to  $K$  **do**

**for**  $i = 1$  to  $n$  **do**

**if**  $i = 1$  **then**

            Use **Theorem 3.1**

            Load  $\hat{\mathbf{W}}^{(k-1,n)}$  and  $\mathbf{R}_{k-1,n}$

            Expand  $\hat{\mathbf{W}}^{(k-1,n)}$  to  $\hat{\mathbf{W}}^{(k-1,n)'}'$

            Obtain activation  $X_{k,1}^{(a)}$  based on  $X_{k,1}^{\text{train}}$  and ViT

            Update  $\mathbf{R}_{k,1}$  by  $X_{k,1}^{(a)}$  and  $\mathbf{R}_{k-1,n}$

            Update  $\mathbf{W}^{(k,1)}$  by  $X_{k,1}^{(a)}$ ,  $Y_{k,1}^{\text{train}}$ ,  $\mathbf{W}^{(k-1,n)'}'$  and  $\mathbf{R}_k$

**else**

            Use **Theorem 3.2**

            Load  $\mathbf{W}^{(k,i-1)}$  and  $\mathbf{R}_{k,i-1}$

            Obtain activation  $X_{k,i}^{(a)}$  based on  $X_{k,i}^{\text{train}}$  and ViT

            Update  $\mathbf{R}_{k,i}$  by  $X_{k,i}^{(a)}$  and  $\mathbf{R}_{k,i-1}$

            Update  $\mathbf{W}^{(k,i)}$  by  $X_{k,i}^{(a)}$ ,  $Y_{k,i}^{\text{train}}$ ,  $\mathbf{W}^{(k,i-1)}$  and  $\mathbf{R}_{k,i-1}$

**end if**

**end for**

**end for**

---

since historical data are not accessible. However, AC can compute the result in a recursive manner, and the recursively updated weight matrix is identical to the joint learning result. Let

$$\mathbf{R}_{1,n-1} = \left( \sum_{i=1}^{n-1} \mathbf{X}_{1,i}^{(a)\text{T}} \mathbf{X}_{1,i}^{(a)} + \gamma \mathbf{I} \right)^{-1} \quad (7)$$

be the *regularized feature autocorrelation matrix* at batch  $n-1$  of task 1, where both historical and current information is encoded in.  $\mathbf{R}_0$  used to update  $\mathbf{R}_{1,1}$  is initialized as an identity matrix at the start of learning. Then we have our solution by the following theorems

**Theorem 3.1** For the batch 1 of task  $k$ , Let  $\hat{\mathbf{W}}^{(k,1)}$  be the optimal estimation. Let  $\hat{\mathbf{W}}^{(k-1,n)'} = [\hat{\mathbf{W}}^{(k-1,n)} \quad \mathbf{0}]$  and  $\hat{\mathbf{W}}^{(k,1)}$  can be calculated via

$$\hat{\mathbf{W}}^{(k,1)} = \hat{\mathbf{W}}^{(k-1,n)'} + \mathbf{R}_{k,1} \mathbf{X}_{k,1}^{(a)\text{T}} \left( \mathbf{Y}_{k,1}^{\text{train}} - \mathbf{X}_{k,1}^{(a)} \hat{\mathbf{W}}^{(k-1,n)'} \right), \quad (8)$$

where

$$\mathbf{R}_{k,1} = \mathbf{R}_{k-1,n} - \mathbf{R}_{k-1,n} \mathbf{X}_{k,1}^{(a)\text{T}} \left( \mathbf{I} + \mathbf{X}_{k,1}^{(a)\text{T}} \mathbf{R}_{k-1,n} \mathbf{X}_{k,1}^{(a)\text{T}} \right)^{-1} \mathbf{X}_{k,1}^{(a)} \mathbf{R}_{k-1,n}. \quad (9)$$

**Theorem 3.2** For the batch  $i$  of task  $k$ , we have

$$\hat{\mathbf{W}}^{(k,i)} = \hat{\mathbf{W}}^{(k,i-1)} + \mathbf{R}_{k,i} \mathbf{X}_{k,i}^{(a)\text{T}} \left( \mathbf{Y}_{k,i}^{\text{train}} - \mathbf{X}_{k,i}^{(a)} \hat{\mathbf{W}}^{(k,i-1)} \right), \quad (10)$$

where

$$\mathbf{R}_{k,i} = \mathbf{R}_{k,i-1} - \mathbf{R}_{k,i-1} \mathbf{X}_{k,i}^{(a)\text{T}} \left( \mathbf{I} + \mathbf{X}_{k,i}^{(a)\text{T}} \mathbf{R}_{k,i-1} \mathbf{X}_{k,i}^{(a)\text{T}} \right)^{-1} \mathbf{X}_{k,i}^{(a)} \mathbf{R}_{k,i-1}. \quad (11)$$

*Proof.* See Appendix A.  $\square$

Thus, we achieve absolute memorization in an exemplar-free way with all data used only once. The learning agenda of AOCIL is summarised in Algorithm 1.

**Data Privacy and Resource Consumption.** Besides identical results with joint learning, AOCIL shows other merits. Compared to replay-based methods, due to its exemplar-free property, AOCIL ensures data privacy by making it impossible to trace back to original data from  $\mathbf{R}_{k,i}$ . In addition,  $\mathbf{R}_{k,i}$  maintains a fixed shape regardless of the input size, and no gradients are needed in the calculation. Thus, AOCIL only requires a small amount of GPU memory for calculation. The total trainable parameters, consisting only of  $\mathbf{R}_{k,i}$  and a linear classifier, take far less time to adjust than tuning the entire network via back-propagation.

## 4. Experiment

To show the effectiveness of AOCIL, we conduct extensive experiments to compare our approach with baseline methods. We build our code based on a survey (Mai et al., 2022) and reproduce relevant results of other methods with ViT as a backbone.

### 4.1. Datasets

We conduct experiments on four real-world benchmark datasets. The first two datasets, CIFAR-100 and CORe50, are commonly used for incremental learning and provide ample samples for each class. To increase the challenge and demonstrate the robustness of our approach, we conduct experiments on additional datasets, FGVCAircraft and DTD, which have limited data for each class and lower inter-class variability.

- **CIFAR-100** (Krizhevsky et al., 2009) is constructed into 10 tasks with disjoint classes, and each task has 10 classes. Each task has 5,000 images for training and 1,000 for testing.

- **CORe50** (Lomonaco & Maltoni, 2017) is a benchmark designed for class incremental learning with 9 tasks and 50 classes: 10 classes in the first task and 5 classes in the subsequent 8 tasks. Each class has 2,398 training images and 900 testing images on average.

- **FGVCAircraft** (Maji et al., 2013) contains 102 different classes of *aircraft models*. 100 classes are selected and divided into 10 tasks. Each class has 33 training images and 33 testing images on average.

- **DTD** (Cimpoi et al., 2014) is a *texture database*, organized into 47 classes. 40 classes are selected and divided into 10

Methods	CIFAR-100			CORe50			FGVCAircraft			DTD		
	<i>Replay-based</i>			<i>Exemplar-free</i>								
Buffer Size	500	1,000	5,000	500	1,000	5,000	500	1,000	5,000	500	1,000	5,000
iCaRL (Rebuffi et al., 2017)	88.6	90.5	91.6	93.5	94.9	95.6	31.6	34.2	36.4	73.2	74.4	74.1
ER (Hayes et al., 2019)	83.0	85.9	90.1	91.7	93.9	94.8	33.6	35.5	35.7	64.5	66.2	65.4
ASER (Shim et al., 2021)	76.7	79.8	87.2	82.9	87.0	87.1	26.2	26.5	25.2	58.1	59.0	57.4
SCR (Mai et al., 2021)	89.5	90.7	91.9	93.3	95.0	95.3	48.7	52.7	55.6	73.8	74.9	75.0
DVC (Gu et al., 2022)	87.5	89.8	<u>92.4</u>	94.0	95.6	<u>97.1</u>	31.8	32.6	33.7	70.0	65.7	67.3
PCR (Lin et al., 2023)	84.1	87.2	89.1	93.8	95.0	95.7	10.7	10.5	10.1	36.3	34.5	35.0
<i>Exemplar-free</i>												
LwF (Li & Hoiem, 2017)	69.3			47.0			14.2			40.2		
EWC (Kirkpatrick et al., 2017)	49.9			47.9			12.0			27.6		
AOCIL	<b>90.6</b> ( $\uparrow$ 21.3)[ $\downarrow$ 1.8]			<b>95.3</b> ( $\uparrow$ 47.4)[ $\downarrow$ 1.8]			<b>61.1</b> ( $\uparrow$ 46.9)[ $\uparrow$ 5.5]			<b>81.6</b> ( $\uparrow$ 41.4)[ $\uparrow$ 6.6]		

Table 1. Comparison on average accuracy among exemplar-free and replay-based methods. Results of other methods are reproduced and modified on the code of (Mai et al., 2022) using the same ViT for a fair comparison. Data in **Bold** are the best within exemplar-free methods, and data underlined are the best considering both categories. Data in “( )” are the difference between AOCIL and the best exemplar-free methods, and “[ ]” are the difference between AOCIL and the best replay-based methods. “ $\uparrow$ ” means leading and “ $\downarrow$ ” means lagging.

tasks. Each class has 40 training images and 40 testing images.

#### 4.2. Evaluation Metrics

We define  $a_{i,j}$  as the accuracy evaluated on the test set of task  $j$  after training the network from task 1 through to  $i$ , and the average accuracy is defined as

$$A_i = \frac{1}{i} \sum_{j=1}^i a_{i,j}. \quad (12)$$

When  $i = K$  (i.e., the total number of tasks),  $A_K$  represents the average accuracy by the end of training.

#### 4.3. Implementation Details

ViT-B (Dosovitskiy et al., 2020), pre-trained on ImageNet-1K (Deng et al., 2009), serves as the backbone network for all methods. The data stream is kept identical across all experiments to ensure a fair comparison. The learning rate and batch size are set to 0.001 and 10, respectively. The optimizer is SGD. We apply three different buffer sizes for replay-based methods. In AOCIL, random projection is applied to project class tokens to a dimension of 1,000. Sigmoid is used to acquire the final activation. The regularization terms are set to be 1. All experiments are conducted on a single RTX 4070ti GPU 12GB, and an average of 3 runs is reported.

#### 4.4. Result Comparison

We compare AOCIL with eight baselines: LwF (Li & Hoiem, 2017), EWC (Kirkpatrick et al., 2017), iCaRL (Rebuffi et al., 2017), ER (Hayes et al., 2019), ASER (Shim et al., 2021), DVC (Gu et al., 2022), PCR (Lin et al., 2023) and SCR (Mai et al., 2021).

Table 1 shows the accuracy results of our approach and all baselines with various buffer sizes. The upper block shows the results of replay-based methods, while the lower block displays the exemplar-free methods.

#### On CIFAR-100 and CORe50

AOCIL is better than other exemplar-free methods. Our approach outperforms the best exemplar-free baseline on each respective dataset by margins of 21.3% and 47.4%.

AOCIL is comparable to those with 1,000 buffer size and surpasses those with 500 buffer size, but gives a slightly worse accuracy compared to replay-based methods with 5,000 buffer size, AOCIL achieves average accuracy of 90.6% on CIFAR-100 and 95.3% on CORe50. When the buffer size is 5,000, the DVC method achieves the highest results of 92.4% and 97.1%, respectively. AOCIL’s performance is within a 1.8% margin of the optimal results and even surpasses several replay-based methods. When the buffer size is 1,000, the margin to the best replay-based method is smaller than 0.3%. In a 500 buffer size situation, AOCIL outperforms all others.

#### On FGVCAircraft and DTD

AOCIL achieves the best results, outperforming 46.9% and 41.4% compared to the best exemplar-free baseline and even leading the best replay-based methods 5.5% and 6.6%, respectively. AOCIL performs 61.1% on FGVCAircraft and 81.6% on DTD, while SCR has the second-best results, which are 55.6% and 75.0%. Other methods show apparent weakness in these two challenging datasets, which have limited training data and less inter-classes variability. The results expose the robustness of our method.

In addition, results on FGVCAircraft and DTD suggest that a larger buffer size does not absolutely lead to higher

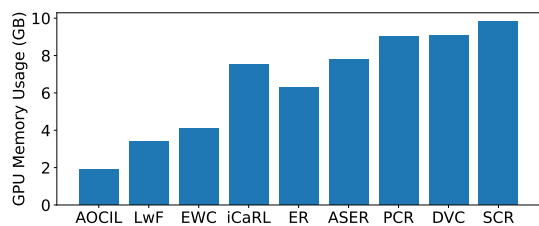


Figure 2. GPU memory consumption in GB with 10 batch size where replay-based methods are with 5,000 buffer size.

Methods	CIFAR-100	CORe50	FGVCAircraft	DTD
LwF	412	877	135	73
EWC	451	922	115	62
iCaRL	832	1,716	53	24
ER	652	1,433	40	21
ASER	5,608	7,700	91	43
SCR	2,843	5,939	88	42
DVC	4,191	9,351	287	130
PCR	1,624	3,742	113	53
AOCIL	<b>261</b>	<b>570</b>	<b>16</b>	<b>8</b>

Table 2. Training time in seconds where replay-based methods are with 5000 buffer size.

accuracy. DVC achieves its best performance with a buffer size of 500 on the DTD dataset, suggesting that a larger buffer size could lead to unnecessary memory usage on small datasets. AOCIL eliminates the difficulty of selecting an appropriate buffer size thanks to its inherent exemplar-free feature.

#### 4.5. Resource Consumption

**GPU Usage.** As shown in Figure 2, AOCIL uses the minimal GPU memory. AOCIL significantly reduces GPU memory usage since it requires no back-propagation, thus gradients are detached from tensors in calculation. This characteristic allows our approach to be applied with larger batch sizes without causing memory leaks. This advantage is particularly beneficial when deploying AOCIL on mobile devices, where memory size is strictly limited.

**Training Time.** Table 2 further illustrates AOCIL’s training time compared to others, highlighting its efficiency. AOCIL is faster than any other baselines on any dataset. Although replay-based methods exhibit a marginal advantage in accuracy over AOCIL on CIFAR-100 and CORe50, time consumption is significantly higher in their approaches than in ours. This merit enables AOCIL’s capability on applications such as autonomous vehicles and real-time surveillance systems requiring fast training.

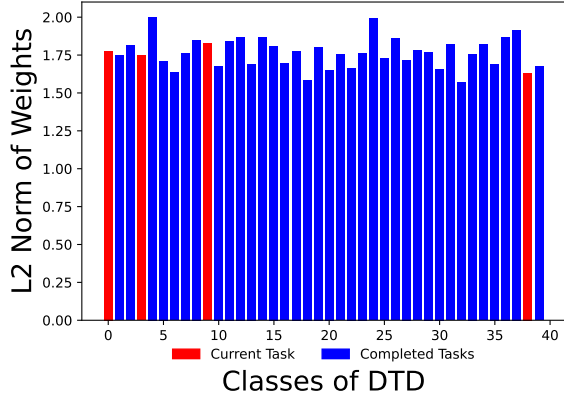


Figure 3. Visualization of the weights of a linear classifier. The result comes from AOCIL on DTD.

#### 4.6. Countering Recency Bias

As demonstrated in Figure 3, the linear classifier of AC obtained through AOCIL training does not exhibit recency bias. Notably, the weights corresponding to the classes in the most recent tasks do not significantly surpass those of the earlier classes. This can be attributed to our utilization of the frozen ViT, which avoids the development of a preference for the most recent classes due to the absence of parameter updates via the loss function. Furthermore, the recursive least square method updates the linear weights with an invariance property, ensuring equal treatment for all samples.

#### 4.7. Ablation Study

As Table 3 shows, we prove the effectiveness of frozen ViT and AC modules. Herein, we define the Online Classifier (OC) as having the identical structure to the AC, but it is updated through back-propagation rather than utilizing the  $R_{k,i}$  and recursive least square. Similarly, we define a Fully Connected Classifier (FCC) (i.e., layer linear classifier) and an Analytic Fully Connected Classifier (AFCC) (i.e., FCC updated by recursive least square). Moreover, the framework must utilize the frozen ViT when employing Analytic Learning. Otherwise, the activations previously encrypted in the  $R_{k,i}$  become meaningless.

We conducted five experiments on the CIFAR-100 and proved that the combination of frozen ViT and AC is crucial with 90.6% accuracy. Without AC, the accuracy drops from 90.6% to 32.1%. Without AC and frozen ViT, a significant reduction in accuracy is observed (e.g., 90.6%  $\rightarrow$  8.4%). Although using AFCC has close results on CIFAR-100, the performance drops on other datasets as Figure 4 shows (Original class token without projection). The results prove that the combination of frozen pre-trained ViT and AC solves the two factors of CF-weakness of back-propagation

Frozen ViT	AC	OC	AFCC	FCC	Result
✓	✓	✗	✗	✗	<b>90.6</b>
✓	✗	✓	✗	✗	32.1
✓	✗	✗	✓	✗	90.5
✓	✗	✗	✗	✓	49.5
✓	✗	✗	✗	✗	49.2
✗	✗	✓	✗	✗	8.4
✗	✗	✗	✗	✓	2.9

Table 3. Average accuracy of CIFAR-100 with different modules combination.

$\gamma$	CIFAR-100	CORe50	FGVCAircraft	DTD
$10^2$	<b>90.6</b>	<b>95.3</b>	55.1	70.3
$10^1$	<b>90.6</b>	<b>95.3</b>	59.5	75.2
1	<b>90.6</b>	<b>95.3</b>	<b>61.1</b>	<b>81.6</b>
$10^{-1}$	90.4	95.2	47.1	81.5
$10^{-2}$	90.1	93.6	34.9	79.1
$10^{-3}$	86.8	89.9	22.4	70.8

Table 4. Average accuracy measured with different regularization terms.

and recency bias.

#### 4.8. Hyperparameter Analysis

**Regularization Term.** Table 4 shows the effects of varying  $\gamma$  and proves  $\gamma=1$  is the suitable choice.

For CIFAR-100 and CORe50, accuracy remains stable from  $\gamma=100$  to  $\gamma=1$ , suggesting resilience to regularization strength within this range. Notably, accuracy drops significantly as  $\gamma$  decreases to 0.001, indicating potential over-fitting at lower  $\gamma$  values due to insufficient regularization.

For FGVCAircraft and DTD, a peak comes at  $\gamma=1$ . Both larger and smaller values lead to significant accuracy reduction.

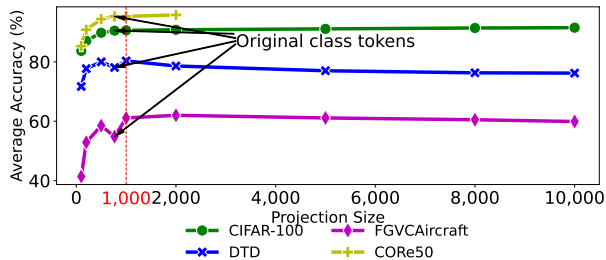


Figure 4. Average accuracy measured in different projection sizes with Sigmoid.

Function	CIFAR-100	CORe50	FGVCAircraft	DTD
Sigmoid	<b>90.6</b>	<b>95.3</b>	<b>61.1</b>	<b>81.6</b>
ReLU	89.8	93.9	53.3	69.5
Tanh	90.5	95.0	58.0	72.9
GELU	89.9	93.9	57.1	70.4

Table 5. Average accuracy on four datasets with different activation functions in 1,000 projection size.

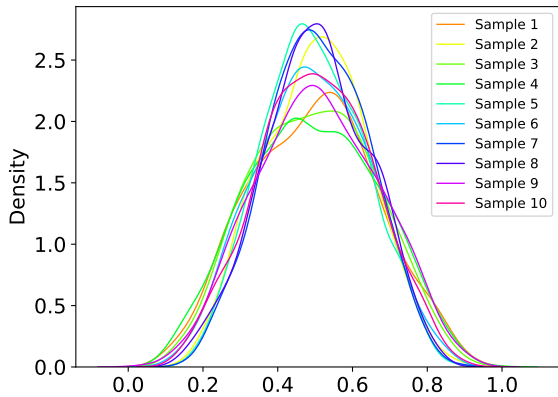


Figure 5. Activation value distribution of a batch on DTD.

**Projection Size.** Figure 4 demonstrates the influence of different random projection sizes and the comparison to using original tokens as input to calculate  $R_{k,i}$ . Our results suggest that the setting of a 1,000-dimensional projection is appropriate. These experiments reveal that higher-dimensional projections may not always improve accuracy, suggesting that projection size must fit the dataset’s volume. If the volume of the dataset is small, a high-dimensional projection results in over-fitting to the training set. The maximum accuracy on DTD is at 1,000 projection size, while the accuracy slightly increases after 1,000. When the projection size is 2,000, the results of FGVCAircraft and CORe50 are a little higher than the results on 1,000, but time consumption is twice higher due to the cubic time complexity in the matrix inverse. Thus, we limit the projection size measurement to 2,000 for CORe50 due to the significant increase in time consumption.

**Activation Function.** Table 5 is measured with a 1,000-dimensional projection. It suggests that the Sigmoid is the best choice based on the average performance. The Sigmoid function’s smooth, bounded output seems particularly beneficial for stabilizing the least squares updates in the chosen dimensional space, leading to a more robust classifier performance than other activation functions.

Moreover, as shown in Figure 5, the Sigmoid activation function tends to produce embedding values that closely

approximate a normal distribution with a mean of 0.5, particularly clustering within a moderate range of 0.3 to 0.7. In Table 5, other activation functions show a significant decrease in performance on small datasets, but Sigmoid maintains a relatively high accuracy. This is likely because its normal distribution helps mitigate model over-fitting. This pattern leads to less fluctuation in model performance across different data points. When projection values are normalized and smoothly distributed, recursive least square provides stable and reliable weight updates and satisfying predictions.

## 5. Conclusion

In this paper, we propose Analytic Online Class Incremental Learning (AOCIL), an exemplar-free method for addressing several limitations of the Online Class Incremental Learning scenario. We use Analytic Learning to acquire the optimal solution of the classifier directly instead of training for dozens of epochs by back-propagation. Leveraging the frozen pre-trained Vision Transformer and the Analytic Classifier updated by recursive least square, our approach achieves the identical solution to joint learning on the whole dataset without preserving any historical exemplars, demonstrating that the approach protects data privacy and reduces resource consumption. Our experiments show that our approach is more accurate than other exemplar-free methods and performs as well as replay-based methods.

## Impact Statements

This paper presents work whose goal is to advance the field of Machine Learning. There are many potential societal consequences of our work, none of which we feel must be specifically highlighted here.

## References

Aljundi, R., Belilovsky, E., Tuytelaars, T., Charlin, L., Caccia, M., Lin, M., and Page-Caccia, L. Online continual learning with maximal interfered retrieval. In *Advances in Neural Information Processing Systems*, pp. 11849–11860, 2019a.

Aljundi, R., Lin, M., Goujaud, B., and Bengio, Y. Gradient based sample selection for online continual learning. In *Advances in Neural Information Processing Systems*, pp. 11816–11825, 2019b.

Cimpoi, M., Maji, S., Kokkinos, I., Mohamed, S., and Vedaldi, A. Describing textures in the wild. In *Proceedings of the IEEE Conference on Computer Vision and Pattern Recognition*, pp. 3606–3613, 2014.

Deng, J., Dong, W., Socher, R., Li, L.-J., Li, K., and Fei-Fei, L. Imagenet: A large-scale hierarchical image database. In *IEEE Computer Society Conference on Computer Vision and Pattern Recognition*, pp. 248–255, 2009.

Dosovitskiy, A., Beyer, L., Kolesnikov, A., Weissenborn, D., Zhai, X., Unterthiner, T., Dehghani, M., Minderer, M., Heigold, G., Gelly, S., et al. An image is worth 16x16 words: Transformers for image recognition at scale. In *International Conference on Learning Representations*, 2020.

Gu, Y., Yang, X., Wei, K., and Deng, C. Not just selection, but exploration: Online class-incremental continual learning via dual view consistency. In *Proceedings of the IEEE/CVF Conference on Computer Vision and Pattern Recognition*, pp. 7442–7451, 2022.

Guo, P., Lyu, M. R., and Mastorakis, N. Pseudoinverse learning algorithm for feedforward neural networks. In *Advances in Neural Networks and Applications*, pp. 321–326, 2001.

Guo, Y., Liu, B., and Zhao, D. Online continual learning through mutual information maximization. In *International Conference on Machine Learning*, pp. 8109–8126. PMLR, 2022.

Hayes, T. L., Cahill, N. D., and Kanan, C. Memory efficient experience replay for streaming learning. In *2019 International Conference on Robotics and Automation*, pp. 9769–9776, 2019.

He, J., Mao, R., Shao, Z., and Zhu, F. Incremental learning in online scenario. In *Proceedings of the IEEE/CVF Conference on Computer Vision and Pattern Recognition*, pp. 13926–13935, 2020.

Hou, S., Pan, X., Loy, C. C., Wang, Z., and Lin, D. Learning a unified classifier incrementally via rebalancing. In *Proceedings of the IEEE/CVF Conference on Computer Vision and Pattern Recognition*, pp. 831–839, 2019.

Kirkpatrick, J., Pascanu, R., Rabinowitz, N., Veness, J., Desjardins, G., Rusu, A. A., Milan, K., Quan, J., Ramalho, T., Grabska-Barwinska, A., et al. Overcoming catastrophic forgetting in neural networks. In *Proceedings of the National Academy of Sciences*, pp. 3521–3526, 2017.

Krizhevsky, A., Hinton, G., et al. Learning multiple layers of features from tiny images. 2009.

Lee, B. H., Jung, O., Choi, J., and Chun, S. Y. Online continual learning on hierarchical label expansion. In *Proceedings of the IEEE/CVF International Conference on Computer Vision*, pp. 11761–11770, 2023.

Li, Z. and Hoiem, D. Learning without forgetting. *IEEE Transactions on Pattern Analysis and Machine Intelligence*, pp. 2935–2947, 2017.

Lin, H., Zhang, B., Feng, S., Li, X., and Ye, Y. Pcr: Proxy-based contrastive replay for online class-incremental continual learning. In *Proceedings of the IEEE/CVF Conference on Computer Vision and Pattern Recognition*, pp. 24246–24255, 2023.

Lomonaco, V. and Maltoni, D. Core50: a new dataset and benchmark for continuous object recognition. In *Conference on Robot Learning*, pp. 17–26, 2017.

Mai, Z., Li, R., Kim, H., and Sanner, S. Supervised contrastive replay: Revisiting the nearest class mean classifier in online class-incremental continual learning. In *Proceedings of the IEEE/CVF Conference on Computer Vision and Pattern Recognition*, pp. 3589–3599, 2021.

Mai, Z., Li, R., Jeong, J., Quispe, D., Kim, H., and Sanner, S. Online continual learning in image classification: An empirical survey. *Neurocomputing*, pp. 28–51, 2022.

Maji, S., Rahtu, E., Kannala, J., Blaschko, M., and Vedaldi, A. Fine-grained visual classification of aircraft. *arXiv preprint arXiv:1306.5151*, 2013.

McCloskey, M. and Cohen, N. J. Catastrophic interference in connectionist networks: The sequential learning problem. In *Psychology of learning and motivation*, volume 24, pp. 109–165. 1989.

Petit, G., Popescu, A., Schindler, H., Picard, D., and Delezoide, B. Fetril: Feature translation for exemplar-free class-incremental learning. In *Proceedings of the IEEE/CVF Winter Conference on Applications of Computer Vision*, pp. 3911–3920, 2023.

Raghu, M., Unterthiner, T., Kornblith, S., Zhang, C., and Dosovitskiy, A. Do vision transformers see like convolutional neural networks? In *Advances in Neural Information Processing Systems*, pp. 12116–12128, 2021.

Rebuffi, S.-A., Kolesnikov, A., Sperl, G., and Lampert, C. H. icarl: Incremental classifier and representation learning. In *Proceedings of the IEEE Conference on Computer Vision and Pattern Recognition*, pp. 2001–2010, 2017.

Shim, D., Mai, Z., Jeong, J., Sanner, S., Kim, H., and Jang, J. Online class-incremental continual learning with adversarial shapley value. In *Proceedings of the AAAI Conference on Artificial Intelligence*, pp. 9630–9638, 2021.

Wang, Q., Wang, R., Wu, Y., Jia, X., and Meng, D. Cba: Improving online continual learning via continual bias adaptor. In *Proceedings of the IEEE/CVF International Conference on Computer Vision*, pp. 19082–19092, 2023.

Wang, Z., Liu, L., Kong, Y., Guo, J., and Tao, D. Online continual learning with contrastive vision transformer. In *European Conference on Computer Vision*, pp. 631–650, 2022.

Wei, Y., Ye, J., Huang, Z., Zhang, J., and Shan, H. Online prototype learning for online continual learning. In *Proceedings of the IEEE/CVF International Conference on Computer Vision*, pp. 18764–18774, 2023.

Zhang, Y., Pfahringer, B., Frank, E., Bifet, A., Lim, N. J. S., and Jia, Y. A simple but strong baseline for online continual learning: Repeated augmented rehearsal. In *Advances in Neural Information Processing Systems*, pp. 14771–14783, 2022.

Zhu, F., Zhang, X.-Y., Wang, C., Yin, F., and Liu, C.-L. Prototype augmentation and self-supervision for incremental learning. In *Proceedings of the IEEE/CVF Conference on Computer Vision and Pattern Recognition*, pp. 5871–5880, 2021.

Zhu, K., Zhai, W., Cao, Y., Luo, J., and Zha, Z.-J. Self-sustaining representation expansion for non-exemplar class-incremental learning. In *Proceedings of the IEEE/CVF Conference on Computer Vision and Pattern Recognition*, pp. 9296–9305, 2022.

Zhuang, H., Lin, Z., and Toh, K.-A. Blockwise recursive moore–penrose inverse for network learning. *IEEE Transactions on Systems, Man, and Cybernetics: Systems*, 52(5):3237–3250, 2021.

Zhuang, H., Weng, Z., Wei, H., Xie, R., Toh, K.-A., and Lin, Z. Acil: Analytic class-incremental learning with absolute memorization and privacy protection. In *Advances in Neural Information Processing Systems*, pp. 11602–11614, 2022.

Zhuang, H., Weng, Z., He, R., Lin, Z., and Zeng, Z. Gkeal: Gaussian kernel embedded analytic learning for few-shot class incremental task. In *Proceedings of the IEEE/CVF Conference on Computer Vision and Pattern Recognition*, pp. 7746–7755, 2023.

## A. Proof of Theorem 3.1 and 3.2

For **Theorem 3.1**, we start with proving the case in batch 1 of task  $k$ .

According to Equation 6, of task  $k - 1$ , we have

$$\hat{\mathbf{W}}^{(k-1,n)} = \left( \sum_{m=1}^{k-1} \sum_{i=1}^n \mathbf{X}_{m,i}^{(a)\top} \mathbf{X}_{m,i}^{(a)} + \gamma \mathbf{I} \right)^{-1} \begin{bmatrix} \mathbf{X}_{1,1}^{(a)\top} \mathbf{Y}_{1,1}^{\text{train}} \\ \vdots \\ \mathbf{X}_{k-1,n}^{(a)\top} \mathbf{Y}_{k-1,n}^{\text{train}} \end{bmatrix}. \quad (13)$$

Hence, at batch 1 of task  $k$ , we have

$$\hat{\mathbf{W}}^{(k,1)} = \left( \sum_{m=1}^{k-1} \sum_{i=1}^n \mathbf{X}_{m,i}^{(a)\top} \mathbf{X}_{m,i}^{(a)} + \gamma \mathbf{I} + \mathbf{X}_{k,1}^{(a)\top} \mathbf{X}_{k,1}^{(a)} \right)^{-1} \begin{bmatrix} \mathbf{X}_{1,1}^{(a)\top} \mathbf{Y}_{1,1}^{\text{train}} \\ \vdots \\ \mathbf{X}_{k-1,n}^{(a)\top} \mathbf{Y}_{k-1,n}^{\text{train}} \\ \mathbf{X}_{k,1}^{(a)\top} \mathbf{Y}_{k,1}^{\text{train}} \end{bmatrix}. \quad (14)$$

We have defined regularized feature autocorrelation matrix  $\mathbf{R}_{k-1,n}$  via

$$\mathbf{R}_{k-1,n} = \left( \sum_{m=1}^{k-1} \sum_{i=1}^n \mathbf{X}_{m,i}^{(a)\top} \mathbf{X}_{m,i}^{(a)} + \gamma \mathbf{I} \right)^{-1} \quad (15)$$

To facilitate subsequent calculations, here we also define a cross-correlation matrix  $\mathbf{Q}_{k-1,n}$

$$\mathbf{Q}_{k-1,n} = \begin{bmatrix} \mathbf{X}_{1,1}^{(a)\top} \mathbf{Y}_{1,1}^{\text{train}} & \cdots & \mathbf{X}_{k-1,n}^{(a)\top} \mathbf{Y}_{k-1,n}^{\text{train}} \end{bmatrix}. \quad (16)$$

Thus, we can rewrite Equation 14 as

$$\hat{\mathbf{W}}^{(k-1,n)} = \mathbf{R}_{k-1,n} \mathbf{Q}_{k-1,n}. \quad (17)$$

Therefore, at batch 1 of task  $k$  we have

$$\hat{\mathbf{W}}^{(k,1)} = \mathbf{R}_{k,1} \mathbf{Q}_{k,1}. \quad (18)$$

From Equation 15 we can recursively calculate  $\mathbf{R}_{k,1}$  from  $\mathbf{R}_{k-1,n}$

$$\mathbf{R}_{k,1} = \left( \mathbf{R}_{k-1,n}^{-1} + \mathbf{X}_{k,1}^{(a)\top} \mathbf{X}_{k,1}^{(a)} \right)^{-1}. \quad (19)$$

According to the Woodbury matrix identity, we have

$$(\mathbf{A} + \mathbf{UCV})^{-1} = \mathbf{A}^{-1} - \mathbf{A}^{-1} \mathbf{U} (\mathbf{C}^{-1} + \mathbf{V} \mathbf{A}^{-1} \mathbf{U})^{-1} \mathbf{V} \mathbf{A}^{-1}. \quad (20)$$

Let  $\mathbf{A} = \mathbf{R}_{k-1,n}^{-1}$ ,  $\mathbf{U} = \mathbf{X}_{k,1}^{(a)\top}$ ,  $\mathbf{C} = \mathbf{I}$ ,  $\mathbf{V} = \mathbf{X}_{k,1}^{(a)}$  in Equation 20, we have

$$\mathbf{R}_{k,1} = \mathbf{R}_{k-1,n} - \mathbf{R}_{k-1,n} \mathbf{X}_{k,1}^{(a)\top} \left( \mathbf{I} + \mathbf{X}_{k,1}^{(a)} \mathbf{R}_{k-1,n} \mathbf{X}_{k,1}^{(a)\top} \right)^{-1} \mathbf{X}_{k,1}^{(a)} \mathbf{R}_{k-1,n}. \quad (21)$$

Hence,  $\mathbf{R}_k$  can be recursively updated using its last task counterpart  $\mathbf{R}_{k-1,n}$  and current data (i.e.,  $\mathbf{X}_{k,1}$ ). This proves the recursive calculation in Equation 9.

Next, we derive the recursive formulation of  $\hat{\mathbf{W}}^{(k,1)}$ . To this end, we also recuse the cross-correlation matrix  $\mathbf{Q}_{k,1}$  at the batch 1 of task  $k$ , i.e.,

$$\mathbf{Q}_{k,1} = \begin{bmatrix} \mathbf{X}_{1,1}^{(a)\top} \mathbf{Y}_{1,1}^{\text{train}} & \cdots & \mathbf{X}_{k-1,n}^{(a)\top} \mathbf{Y}_{k-1,n}^{\text{train}} & \mathbf{X}_{k,1}^{(a)\top} \mathbf{Y}_{k,1}^{\text{train}} \end{bmatrix} = \mathbf{Q}'_{k-1,n} + \mathbf{X}_{k,1}^{(a)\top} \mathbf{Y}_{k,1}^{\text{train}}. \quad (22)$$

where

$$\mathbf{Q}'_{k-1,n} = [\mathbf{Q}_{k-1,n} \quad \mathbf{0}_{d_{(a)} \times d_{y_k}}] \quad (23)$$

where  $d_{(a)}$  is the dimension of activation and  $d_{y_k}$  is dimension of total classes of task  $k$ . Note that the concatenation in Equation 23 is due to fact that  $\mathbf{Y}_{k,1}$  of task  $k$  contains more data classes (hence more columns) than  $\mathbf{Y}_{k-1,n}$ .

Let  $\mathbf{K}_{k,1} = (\mathbf{I} + \mathbf{X}_{k,1}^{(a)} \mathbf{R}_{k-1,n} \mathbf{X}_{k,1}^{(a)\top})^{-1}$ . Since  $\mathbf{I} = \mathbf{K}_{k,1} \mathbf{K}_{k,1}^{-1} = \mathbf{K}_{k,1} (\mathbf{I} + \mathbf{X}_{k,1}^{(a)} \mathbf{R}_{k-1,n} \mathbf{X}_{k,1}^{(a)\top})$ , we have  $\mathbf{K}_{k,1} = \mathbf{I} - \mathbf{K}_{k,1} \mathbf{X}_{k,1}^{(a)} \mathbf{R}_{k-1,n} \mathbf{X}_{k,1}^{(a)\top}$ . Therefore,

$$\begin{aligned} \mathbf{R}_{k-1,n} \mathbf{X}_{k,1}^{(a)\top} (\mathbf{I} + \mathbf{X}_{k,1}^{(a)} \mathbf{R}_{k-1,n} \mathbf{X}_{k,1}^{(a)\top})^{-1} &= \mathbf{R}_{k,1} \mathbf{X}_{k,1}^{(a)\top} \mathbf{K}_{k,1} \\ &= \mathbf{R}_{k,1} \mathbf{X}_{k,1}^{(a)\top} (\mathbf{I} - \mathbf{K}_{k,1} \mathbf{X}_{k,1}^{(a)} \mathbf{R}_{k-1,n} \mathbf{X}_{k,1}^{(a)\top}) \\ &= (\mathbf{R}_{k-1,n} - \mathbf{R}_{k-1,n} \mathbf{X}_{k,1}^{(a)\top} \mathbf{K}_{k,1} \mathbf{X}_{k,1}^{(a)} \mathbf{R}_{k-1,n}) \mathbf{X}_{k,1}^{(a)\top} \\ &= \mathbf{R}_{k,1} \mathbf{X}_{k,1}^{(a)\top}. \end{aligned} \quad (24)$$

As  $\hat{\mathbf{W}}^{(k-1,n)'} = [\hat{\mathbf{W}}^{(k-1,n)} \quad \mathbf{0}]$  has expanded its dimension similar to what  $\mathbf{Q}'_{k-1,n}$  does, we have

$$\hat{\mathbf{W}}^{(k-1,n)'} = \mathbf{R}_{k-1,n} \mathbf{Q}'_{k-1,n}. \quad (25)$$

Hence,  $\hat{\mathbf{W}}^{(k,1)}$  can be rewritten as

$$\hat{\mathbf{W}}^{(k,1)} = \mathbf{R}_{k,1} \mathbf{Q}_{k,1} = \mathbf{R}_{k,1} (\mathbf{Q}'_{k-1,n} + \mathbf{X}_{k,1}^{(a)\top} \mathbf{Y}_{k,1}^{\text{train}}) = \mathbf{R}_{k,1} \mathbf{Q}'_{k-1,n} + \mathbf{R}_{k,1} \mathbf{X}_{k,1}^{(a)\top} \mathbf{Y}_{k,1}^{\text{train}}. \quad (26)$$

By substituting Equation 21 into  $\mathbf{R}_{k,1} \mathbf{Q}'_{k-1,n}$ , we have

$$\begin{aligned} \mathbf{R}_{k,1} \mathbf{Q}'_{k-1,n} &= \mathbf{R}_{k-1,n} \mathbf{Q}'_{k-1,n} - \mathbf{R}_{k-1,n} \mathbf{X}_{k,1}^{(a)\top} (\mathbf{I} + \mathbf{X}_{k,1}^{(a)} \mathbf{R}_{k-1,n} \mathbf{X}_{k,1}^{(a)\top})^{-1} \mathbf{X}_{k,1}^{(a)} \mathbf{R}_{k-1,n} \mathbf{Q}'_{k-1,n} \\ &= \hat{\mathbf{W}}^{(k-1,n)'} - \mathbf{R}_{k-1,n} \mathbf{X}_{k,1}^{(a)\top} (\mathbf{I} + \mathbf{X}_{k,1}^{(a)} \mathbf{R}_{k-1,n} \mathbf{X}_{k,1}^{(a)\top})^{-1} \mathbf{X}_{k,1}^{(a)} \hat{\mathbf{W}}^{(k-1,n)'} . \end{aligned} \quad (27)$$

According to Equation 24, Equation 27 can be rewritten as

$$\mathbf{R}_{k,1} \mathbf{Q}'_{k-1,n} = \hat{\mathbf{W}}^{(k-1,n)'} - \mathbf{R}_{k,1} \mathbf{X}_{k,1}^{(a)\top} \mathbf{X}_{k,1}^{(a)} \hat{\mathbf{W}}^{(k-1,n)'} . \quad (28)$$

By inserting Equation 27 into Equation 26, we have

$$\begin{aligned} \hat{\mathbf{W}}^{(k,1)} &= \hat{\mathbf{W}}^{(k-1,n)'} - \mathbf{R}_{k,1} \mathbf{X}_{k,1}^{(a)\top} \hat{\mathbf{W}}^{(k-1,n)'} + \mathbf{R}_{k,1} \mathbf{X}_{k,1}^{(a)\top} \mathbf{Y}_{k,1}^{\text{train}} \\ &= \hat{\mathbf{W}}^{(k-1,n)'} + \mathbf{R}_{k,1} \mathbf{X}_{k,1}^{(a)\top} (\mathbf{Y}_{k,1}^{\text{train}} - \mathbf{X}_{k,1}^{(a)} \hat{\mathbf{W}}^{(k-1,n)'}) , \end{aligned} \quad (29)$$

which proves the case in the batch 1 of task  $k$ .

For **Theorem 3.2**, we consider the case at rest batches of task  $k$ . In the rest of batches, the number of classes maintain unchanged compared with batch 1, which means no column expansion is required. According to Equation 29, we substitute  $\hat{\mathbf{W}}^{(k-1,n)'}$  by  $\hat{\mathbf{W}}^{(k,i-1)}$ . Similar substitution is applied to  $\mathbf{R}_{k-1,n}$  with  $\mathbf{R}_{k,i-1}$  according to Equation 21 since the shape of regularized feature autocorrelation matrix is remained through whole learning agenda. Then we have

$$\hat{\mathbf{W}}^{(k,i)} = \hat{\mathbf{W}}^{(k,i-1)} + \mathbf{R}_{k,i} \mathbf{X}_{k,i}^{(a)\top} (\mathbf{Y}_{k,i}^{\text{train}} - \mathbf{X}_{k,i}^{(a)} \hat{\mathbf{W}}^{(k,i-1)}), \quad (30)$$

$$\mathbf{R}_{k,i} = \mathbf{R}_{k,i-1} - \mathbf{R}_{k,i-1} \mathbf{X}_{k,i}^{(a)\top} (\mathbf{I} + \mathbf{X}_{k,i}^{(a)} \mathbf{R}_{k,i-1} \mathbf{X}_{k,i}^{(a)\top})^{-1} \mathbf{X}_{k,i}^{(a)} \mathbf{R}_{k,i-1}, \quad (31)$$

which complete the proof.  $\square$